Supplementary Information

Predicting Intersystem Crossing Efficiencies of Organic Molecules for Efficient Thermally Activated Delayed Fluorescence

Shen Xu,[a] Qingqing Yang,[a] Yifang Wan,[a] Runfeng Chen,*[a] Shuang Wang,[a] Yubing Si,*[b] Baocheng Yang,[b] Dan Liu,[c] Chao Zheng [a] and Wei Huang *[a c]

[a] Key Laboratory for Organic Electronics and Information Displays & Jiangsu Key Laboratory for Biosensors, Institute of Advanced Materials (IAM), Jiangsu National Synergistic Innovation Center for Advanced Materials (SICAM), Nanjing University of Posts & Telecommunications, 9 Wenyuan Road, Nanjing 210023, People's Republic of China.

[b] Henan Key Laboratory of Nanocomposites and Applications, Institute of Nanostructured Functional Materials, Huanghe Science and Technology College, Zhengzhou 450006, People's Republic of China.

[c] Shaanxi Institute of Flexible Electronics (SIFE), Northwestern Polytechnical University (NPU), 127 West Youyi Road, Xi'an, 710072, People's Republic of China

E-mail: iamrfchen@njupt.edu.cn; yubingsi@infm.hhstu.edu.cn; iamwhuang@njupt.edu.cn.

This file includes:

Figure S1: Potential energy surface of S_0, S_1 and T_1.

Figure S2: Absolute deviation of E_{S1}, E_{T1} and ΔE_{ST} of 7 different functionals against experimental values.

Figure S3: Empirical relation between the experimental k_{ISC} and calculated $\Delta\alpha_n$.

Figure S4: Empirical relation between the experimental k_{ISC} and calculated $|s_H\text{-}s_L|$.

Table S1: Absolute variation of Calculated E_{S1}, E_{T1}, ΔE_{ST} using different functionals against Experimental Data.

Table S2: Dihedral angles between the donor and acceptor units at S_1 and T_1 states as well as the dihedral angle changes during the $S_1 \leftrightarrow T_1$ transition of investigated TADF molecules.

Tables S3–S8: Calculated configuration proportion α_n% of HONTO for S_1, T_1 and T_2 state based on MPA of **ACRFLCN**, **DMAC-DPS**, **2CzPN**, **ACRXTN**, **Ac-OPO** and **Ac-OSO.**

Tables S9–S10: Calculated $|s_H+s_L|$ (%) based on NTO analysis of S_0 geometry and $|s_H\text{-}s_L|$ (%) based on NTO analysis of T_1 geometry.

Tables S11–S16: Calculated transition configuration of S_1 and T_1-T_3 for **ACRFLCN**, **DMAC-DPS**, **2CzPN**, **ACRXTN**, **Ac-OPO** and **Ac-OSO**.

Computational Methodology

The density functional theory (DFT) and time-dependent density functional dependent theory (TD-DFT) calculations were performed to investigate the singlet/triplet exciton transformation using Gaussian 09 package.[1] The Becker's three-parameter exchange functional[2] along with the Lee Yang Parr's correlation functional[3] (B3LYP) that can well predict the geometric structures of organic molecules, was adopted to optimize the ground state (S_0) geometries of all molecules in assistant with the 6-31G(d) basis set. The optimized structures were further characterized by harmonic vibrational frequency analysis to confirm that real local minima without any imaginary frequency was reached at the same computational level. As for excited states, TDDFT/B3LYP/6-31G* and unrestricted DFT (UDFT)/B3LYP/6-31G* were used to optimize geometries of lowest singlet excited state (S_1) and lowest singlet excited state (T_1), respectively, and to calculate their energies. Since the configurations of charge-transfer (CT) characteristics are related to different HF exchange percentage, exchange-correlation (XC) functionals, including B3LYP (20% HF), PBE0 (25% HF), BMK (42% HF), M06-2X (56% HF), and M06-HF (100% HF) functionals, as well as long-range functionals of ωB97XD and CAM-B3LYP, were investigated. B3LYP functional was selected eventually owing to the smallest absolute deviation between theoretical and experimental values.

To get further insights into the nature of the excited states, natural transition orbitals (NTOs) analysis was performed based on TD-DFT results to offer a compact orbital representation for the electronic transition density matrix. In addition, using the overlap integral function embedded in Multiwfn[4], the overlap integrals of $I_{S/T}$ between the highest occupied NTO (HONTO) and the lowest unoccupied NTO (LUNTO) of investigated molecules can be calculated. To identify proportion of (n, π^*) configuration (α_n%) of the excited states, Mulliken population analysis (MPA) was performed to calculate the n orbital components with the aid of Multiwfn package. Electron density differences (EDD) from S_0 to S_1 and S_0 to T_n based on optimized S_0 geometries was also performed in the assistant of Multiwfn package. Following the previously developed calculation method of charge transfer amount, excited state similarity in HONTO (s_H) and LUNTO (s_L) between the singlet and triplet excited states can be calculated according to equation:

$$S_{H/L} = 1 - \frac{\sum_i |a_i - b_i|}{2} \quad (1)$$

where $\sum_i a_i = 1$ and $\sum_i b_i = 1$. The index i is the number of atoms in the molecule; a_i and b_i are the contribution percentages of different atoms in the frontier NTO of the corresponding singlet and triplet excited states, respectively. This orbital composition analysis was done by using Multiwfn.[4] $|a_i\text{-}b_i|$ denotes the contribution percentage difference of an atom (i) in the HONTO (or LUNTO) between the singlet and triplet excited states.

Based on B3LYP functional and cc-pVDZ basis set, spin-orbit coupling (SOC) matrix

elements between the singlet and triplet excited states are calculated with quadratic response function methods using the Dalton program.[5] The process of intersystem crossing (ISC) and reverse intersystem crossing (RISC) can be described as:

$$M^S + M^0 \rightarrow M^0 + M^T \quad (2)$$

$$M^T + M^0 \rightarrow M^0 + M^S \quad (3)$$

where M^0 is the ground state molecule interacting with the neighboring excited singlet or triplet molecule (M^S/M^T) to transfer the energy between them. Therefore, the ISC or RISC reorganization energy ($\lambda_{in,\ ISC/RISC}$), in principle, can be calculated in equations 4 and 5:

$$\lambda_{in}^{ISC} = E^T(M^S) - E^T(M^T) \quad (4)$$

$$\lambda_{in}^{RISC} = E^S(M^T) - E^S(M^S) \quad (5)$$

Here, $E^T(M^S)$ and $E^T(M^T)$ are the total energies of the triplet species under the optimum geometry of M^S and M^T, respectively; $E^S(M^T)$ and $E^S(M^S)$ represent the total energies of the singlet molecule under the optimum geometry of M^T and M^S, respectively.

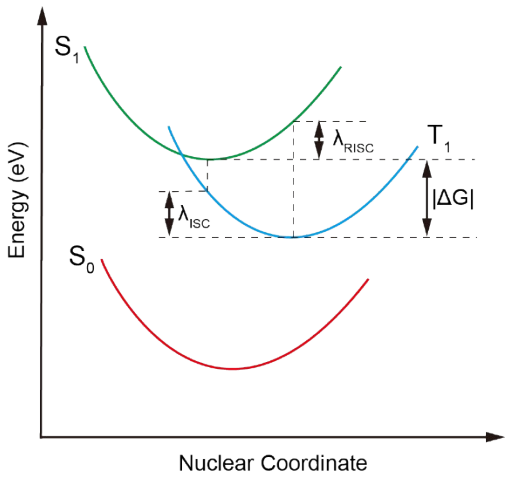

Fig. S1 Potential energy surface of S_0, S_1 and T_1.

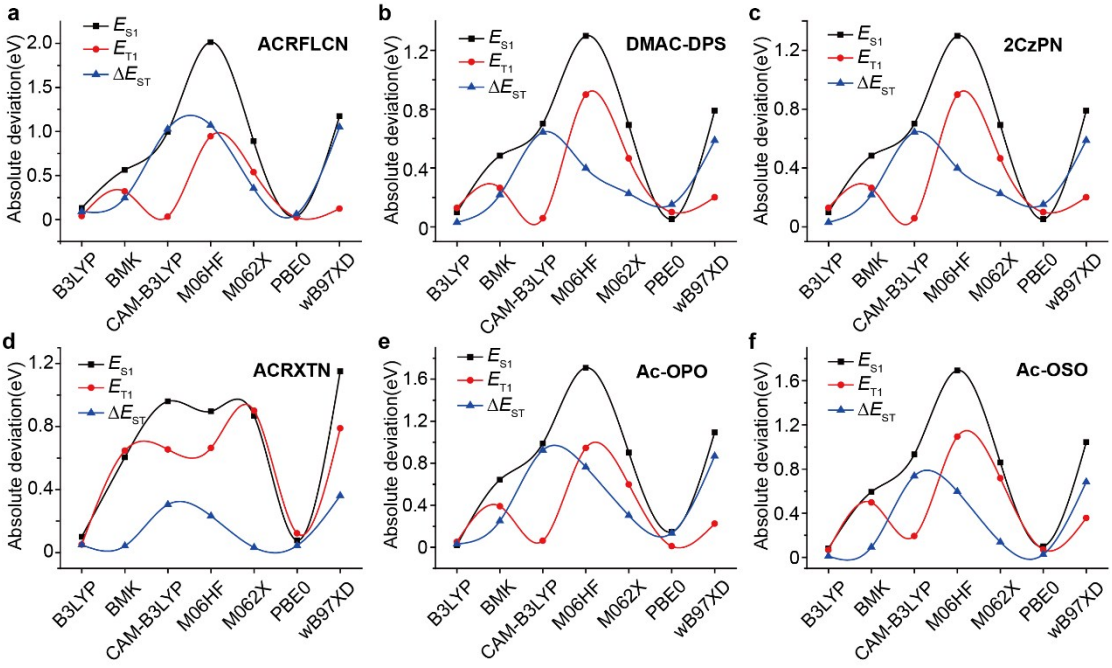

Fig. S2 Absolute deviation of E_{S1}, E_{T1} and ΔE_{ST} of 7 different functionals against experimental values.

Table S1 Absolute variation of Calculated E_{S1}, E_{T1}, ΔE_{ST} using different functionals against Experimental Data.

Functionals	$E_S/E_T/\Delta E_{ST}$(eV)					
	ACRFLCN	**DMAC-DPS**	**2CzPN**	**ACRXTN**	**Ac-OPO**	**Ac-OSO**
B3LYP	2.55/2.54/0.01	2.73/2.72/0.01	2.84/2.50/0.34	2.43/2.42/0.01	3.09/3.03/0.06	2.94/2.89/0.05
BMK	3.24/2.90/0.34	3.39/3.38/0.02	3.42/2.89/0.53	3.13/3.12/0.02	3.75/3.47/0.28	3.61/3.46/0.16
CAM-B3LYP	3.68/2.55/1.13	3.70/3.13/0.57	3.64/2.69/0.95	3.49/3.13/0.36	4.10/3.14/0.96	3.95/3.15/0.80
M06HF	4.69/3.52/1.17	4.27/3.83/0.44	4.24/3.53/0.71	3.43/3.13/0.29	4.82/4.02/0.79	4.71/4.05/0.66
M062X	3.57/3.12/0.45	3.61/3.59/0.02	3.63/3.10/0.54	3.40/3.37/0.03	4.01/3.68/0.33	3.88/3.68/0.20
PBE0	2.72/2.56/0.16	2.89/2.88/0.02	2.99/2.53/0.46	2.61/2.59/0.02	3.25/3.09/0.16	3.12/3.03/0.09
ωB97X-D	3.85/2.70/1.15	3.85/3.27/0.58	3.73/2.83/0.90	3.68/3.26/0.42	4.20/3.31/0.89	4.06/3.32/0.75

Table S2 Donor-acceptor dihedral angles of S_1, T_1 and their differences of investigated molecules.

Molecule	Dihedral angle (°)		Dihedral angle change (°)
	S_1	T_1	
Ac-OPO	91.98	83.62	8.36
Ac-OSO	86.41	83.84	2.57
ACRXTN	90.02	90.09	0.07
DMAC-DPS	89.83	89.87	0.04
ACRFLCN	102.97	102.26	0.71
2CzPN	52.27	51.97	0.30

Table S3 Calculated configuration proportion α_n% of HONTO for S_1, T_1 and T_2 state based on MPA of **ACRFLCN.**

Atom	Basis	α_n^i(HONTO)		
		S_1	T_1	T_2
10(N)	P_Y	27.04%	-	26.94%
28(N)	P_Z	-	6.69%	-
30(N)	P_Z	-	6.69%	-

Table S4 Calculated configuration proportion α_n% of HONTO for S_1, T_1 and T_2 state based on MPA of **DMAC-DPS.**

Atom	Basis	α_n^i(HONTO)		
		S_1	T_1	T_2
24(N)	P_Z	28.39%	-	28.47%
46(N)	P_X	-	2.29%	-
46(N)	P_Y	-	0.90%	-
46(N)	P_Z	-	20.30%	-

Table S5 Calculated configuration proportion α_n% of HONTO for S_1, T_1 and T_2 state based on MPA of **2CzPN.**

Atom	Basis	α_n^i(HONTO)		
		S_1	T_1	T_2
8(N)	P_Z	-	3.61%	0.56%
10(N)	P_Z	-	3.61%	0.56%
13(N)	P_X	3.08%	2.61%	2.60%
13(N)	P_Y	2.37%	1.76%	2.67%
13(N)	P_Z	6.06%	5.39%	6.15%
34(N)	P_X	3.08%	2.61%	2.60%
34(N)	P_Y	2.37%	1.76%	2.67%
34(N)	P_Z	6.05%	5.39%	6.15%

Table S6 Calculated configuration proportion α_n% of HONTO for S_1, T_1 and T_2 state based on MPA of **ACRXTN.**

Atom	Basis	α_n^i(HONTO)		
		S_1	T_1	T_2
15(O)	P_X	-	-	67.73%
15(O)	P_Y	-	3.21%	0.73%
15(O)	P_Z	-	1.79%	8.84%

23(N)	P_X	0.63%	0.55%	-
23(N)	P_Y	0.90%	0.62%	-
23(N)	P_Z	24.74%	22.35%	-

Table S7 Calculated configuration proportion α_n% of HONTO for S_1, T_1 and T_2 state based on MPA of **Ac-OPO.**

Atom	Basis	α_n^i(HONTO)		
		S_1	T_1	T_2
23(N)	P_X	2.15%	2.10%	1.17%
23(N)	P_Y	2.91%	2.83%	2.23%
23(N)	P_Z	21.13%	20.54%	16.20%

Table S8 Calculated configuration proportion α_n% of HONTO for S_1, T_1 and T_2 state based on MPA of **Ac-OSO.**

Atom	Basis	α_n^i(HONTO)		
		S_1	T_1	T_2
23(N)	P_X	0.86%	0.86%	0.66%
23(N)	P_Z	24.89%	24.76%	18.34%

Table S9 $|s_H+s_L|$ (%) calculated based on NTO analysis of S_0 geometry.

Transitions	**ACRFLCN**	**DMAC-DPS**	**2CzPN**	**ACRXTN**	**Ac-OPO**	**Ac-OSO**
$S_1 \rightarrow T_1$	198.6	196.8	172.7	199.1	186.4	193.6
$S_1 \rightarrow T_2$	101.5	199.6	178.8	85.6	126.1	137.1

Table S10 $|s_H-s_L|$ (%) calculated based on NTO analysis of T_1 geometry.

Transitions	**ACRFLCN**	**DMAC-DPS**	**2CzPN**	**ACRXTN**	**Ac-OPO**	**Ac-OSO**
$S_1 \rightarrow T_1$	90.3	65.3	32.2	12.3	9.4	2.7
$S_1 \rightarrow T_2$	0.1	0.5	24.3	70.5	73.7	81.5

Table S11 Calculated transition configuration of S_1 and T_1-T_3 for **ACRFLCN.**

Excited State	Energy (eV)	Transition configuration (%)
S_1	2.5493	H→L(99.72)
T_1	2.541	H→L(99.56)
T_2	2.6532	H-8→L+1(2.33);H-3→L(17.5);H-1→L(71.36)
T_3	3.1841	H-4→L+9(4.12);H-3→L+5(3.16);H-2→L+8(4.44); H-1→L+5(3.31);H→L+2(49.07);H→L+6(8.11); H→L+7(23.85)

Table S12 Calculated transition configuration of S_1 and T_1-T_3 for **DMAC-DPS.**

Excited State	Energy (eV)	Transition configuration (%)
S_1	2.7309	H-1→L+2(5.06);H→L(93.94)
T_1	2.7202	H-1→L+2(5.38);H→L(93.5)
T_2	2.7209	H-1→L(93.46);H→L+2(5.4)
T_3	3.14	H-5→L+4(2);H-4→L+5(2.01);H-1→L+3(16.38); H-1→L+7(19.49);H→L+1(30.67);H→L+6(21.11)

Table S13 Calculated transition configuration of S_1 and T_1-T_3 for **2CzPN.**

Excited State	Energy (eV)	Transition configuration (%)
S_1	2.8503	H→L(99.07)
T_1	2.5082	H-8→L(2.35);H-6→L(8.4);H→L(83.71)
T_2	2.7144	H-1→L(95.96)
T_3	3.0042	H-3→L+2(9.96);H-2→L(69.33);H-2→L+3(9.73)

Table S14 Calculated transition configuration of S_1 and T_1-T_3 for **ACRXTN**.

Excited State	Energy (eV)	Transition configuration (%)
S_1	2.4298	H→L(97.87)
T_1	2.4187	H→L(97.58)
T_2	3.0795	H-7→L(7.35);H-4→L(4.06);H-3→L(2.78);H-1→L(81.45)
S_2	3.5324	H→L+1(95)

Table S15 Calculated transition configuration of S_1 and T_1-T_3 for **Ac-OPO.**

Excited states	Energy (eV)	Transition configuration (%)
S_1	3.088	H→L(97.07)
T_1	3.0272	H→L(87.36);H→L+2(3.49);H→L+7(5.01)
T_2	3.2475	H-4→L+9(2.65);H-3→L+6(3.65);H-1→L+8(3.21)H→L(6.25); H→L+1(35.18); H→L+2(4.95);H→L+5(3.23);H→L+7(36.8)
T_3	3.2933	H-3→L+6(2.55);H-1→L+8(2.44);H→L(2.07);H→L+1(53.57); H→L+7(30.73)

Table S16 Calculated transition configuration of S_1 and T_1-T_3 for **Ac-OSO.**

Excited states	Energy (eV)	Transition configuration (%)
S_1	2.9404	H→L(93.62);H→L+1(2.7);H→L+2(3.36)
T_1	2.8934	H→L(89.58);H→L+1(2.66);H→L+2(5.08)
T_2	3.2382	H→L+1(72.67);H→L+2(9.2);H→L+3(5.21);H→L+5(9.11)
T_3	3.2744	H-4→L+7(4.2);H-2→L+4(6.01);H-1→L+6(5.58);H→L(3.91); H→L+1(12.47); H→L+5(63.34)

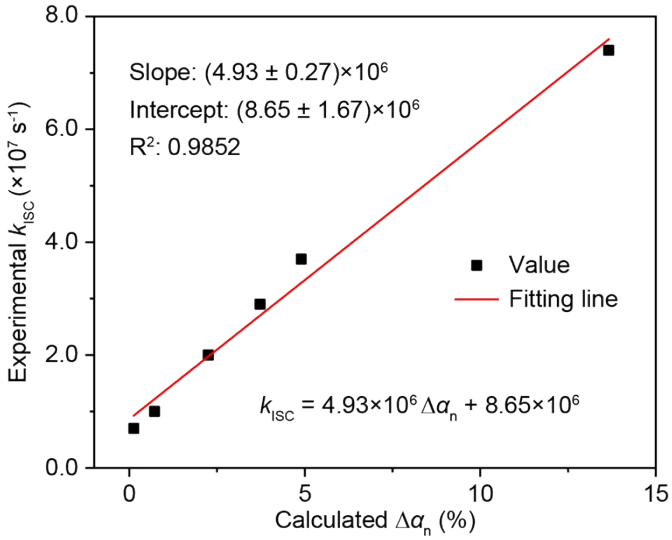

Fig. S3 Empirical relation between the experimental k_{ISC} and calculated $\Delta\alpha_n$.

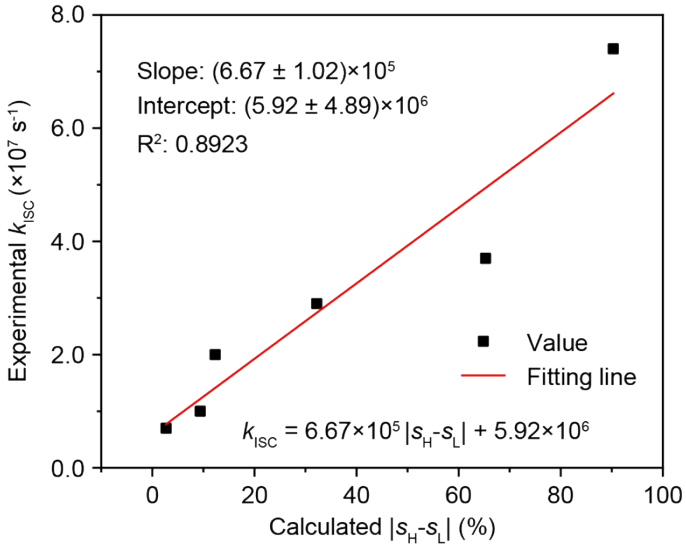

Fig. S4 Empirical relation between the experimental k_{ISC} and calculated $|s_H\text{-}s_L|$.

References

1 M. J. Frisch, G. W. Trucks, H. B. Schlegel, G. E. Scuseria, M. A. Robb, J. R. Cheeseman, G. Scalmani, V. Barone, B. Mennucci, G. A. Petersson, H. Nakatsuji, M. Caricato, X. Li, H. P. Hratchian, A. F. Izmaylov, J. Bloino, G. Zheng, J. L. Sonnenberg, M. Hada, M. Ehara, K. Toyota, R. Fukuda, J. Hasegawa, M. Ishida, T. Nakajima, Y. Honda, O. Kitao, H. Nakai, T. Vreven, J. A. Montgomery Jr., J. E. Peralta, F. Ogliaro, M. Bearpark, J. J. Heyd, E. Brothers, K. N. Kudin, V. N. Staroverov, R. Kobayashi, J. Normand, K. Raghavachari, A. Rendell, J. C. Burant, S. S. Iyengar, J. Tomasi, M. Cossi, N. Rega, J. M. Millam, M. Klene, J. E. Knox, J. B. Cross, V. Bakken, C. Adamo, J. Jaramillo, R. Gomperts, R. E. Stratmann, O. Yazyev, A. J. Austin, R. Cammi, C. Pomelli, J. W. Ochterski, R. L. Martin, K. Morokuma, V. G. Zakrzewski, G. A. Voth, P. Salvador, J. J. Dannenberg, S. Dapprich, A. D. Daniels, O. Farkas, J. B. Foresman, J. V. Ortiz, J. Cioslowski and D. J. Fox, *Gaussian 09 (Gaussian, Inc., Wallingford, CT)*, 2009 **Vol. 1**.

2 A. D. Becke, *J. Chem. Phys.*, 1993, **98**, 5648.

3 C. T. Lee, W. T. Yang and R. G. Parr, *Phys. Rev. B*, 1988, **37**, 785.

4 T. Lu and F. Chen, *J. Comput. Chem.*, 2012, **33**, 580.

5 K. Aidas, C. Angeli, K. L. Bak, V. Bakken, R. Bast, L. Boman, O. Christiansen, R. Cimiraglia, S. Coriani, P. Dahle, E. K. Dalskov, U. Ekstrom, T. Enevoldsen, J. J. Eriksen, P. Ettenhuber, B. Fernandez, L. Ferrighi, H. Fliegl, L. Frediani, K. Hald, A. Halkier, C. Hattig, H. Heiberg, T. Helgaker, A. C. Hennum, H. Hettema, E. Hjertenaes, S. Host, I. Hoyvik, M. F. Iozzi, B. Jansik, H. J. A. Jensen, D. Jonsson, P. Jorgensen, J. Kauczor, S. Kirpekar, T. Kjrgaard, W. Klopper, S. Knecht, R. Kobayashi, H. Koch, J. Kongsted, A. Krapp, K. Kristensen, A. Ligabue, O. B. Lutnaes, J. I. Melo, K. V. Mikkelsen, R. H. Myhre, C. Neiss, C. B. Nielsen, P. Norman, J. Olsen, J. M. H. Olsen, A. Osted, M. J. Packer, F. Pawlowski, T. B. Pedersen, P. F. Provasi, S. Reine, Z. Rinkevicius, T. A. Ruden, K. Ruud, V. V. Rybkin, P. Salek, C. C. M. Samson, A. S. de Meras, T. Saue, S. P. A. Sauer, B. Schimmelpfennig, K. Sneskov, A. H. Steindal, K. O. Sylvester-Hvid, P. R. Taylor, A. M. Teale, E. I. Tellgren, D. P. Tew, A. J. Thorvaldsen, L. Thogersen, O. Vahtras, M. A. Watson, D. J. D. Wilson, M. Ziolkowski and H. Agren, *Wires. Comput. Mol. Sci.*, 2014, **4**, 269.